

TESTING AND ANALYSIS OF LOW PRESSURE, TRANSPARENT TUBE SOLAR RECEIVER FOR THE SUNSPOT CYCLE

J. Hoffmann^{1,*}, C. van der Merwe¹

ABSTRACT

This paper proposes a low pressure tubular solar receiver for a solarized gas turbine. The receiver comprises of concentric tubes with a transparent outer tube, and the annular space is filled with a porous medium. Air is heated by concentrated solar radiation as it flows through the porous medium. To proof our concept, a single 1.5 m long tube was tested on an existing eight mirror linear Fresnel collector, and test data is documented. A temperature increase of about 40 °C was recorder for a concentration ratio of 7:1 and superficial velocity of 1 m/s. Volumetric absorption was a disappointingly low 28 %, mainly due to the low packing factor and reflection of sunlight from the tube's outer surface. A computational fluid dynamics (CFD) model of the test set-up was used to extract the extinction and absorption coefficients of the porous medium, by fitting a quadratic response surface through the mean square errors between experimental and CFD data. Our analysis indicates that we can increase receiver efficiency significantly through raising the packing factor and applying an anti-reflection coating to the tube surface.

Keywords: *Low Pressure Solar Receiver, Transparent Tube, Linear Fresnel, Porous Medium*

INTRODUCTION

The SUNSPOT cycle [1] aims to generate electricity at utility scale almost continuously from solar radiation. It aims to use the potentially high efficiency of a Brayton cycle during daytime operation, combined with a bottoming Rankine cycle. Air is pre-heated in the central solar receiver, augmented by a combustion chamber to ensure high turbine inlet temperatures. Hot exhaust gases from the gas turbine is passed through a rock bed thermal energy storage system for night-time use. At night, heat is extracted from the rock bed thermal energy storage to generate steam for the Rankine cycle.

Reaching high temperatures in the receiver has been a challenge. Lubkoll et al [2] proposed the spiked concept air preheater, whilst a hybrid receiver [3, 4, 5] were also considered specifically for the SUNSPOT cycle and its variants. In both cases the incident heat flux, and ultimately air temperature is limited by the tube wall temperature.

Existing solar thermal power plants use either thermal oils, molten salt or water/steam as heat transfer fluid. In the case of thermal oil and molten salt, the receiver temperature is effectively limited by the decomposition of the heat transfer fluid, whilst pressure is limiting the maximum operating conditions in direct steam plant. In plant using air as heat transfer fluid, the maximum temperature is imposed by structural material limits. The problem is aggravated by poor heat transfer on the air side, as numerous papers on heat transfer enhancement inside tubes [6, 7, 8] attested.

Achieving high temperature at high pressure has been an elusive goal, as recent reviews by Ávila-Marín [9] and Ho and Iverson [10] attested. Prototypes capable of reaching temperatures above 1 000 °C at pressures up to 20 bar have been demonstrated, albeit in the kilowatt, rather than megawatt range. These receivers typically make use of a volumetric absorber behind a pressurized dome-shaped quartz window. The most successful in achieving high temperature, seems to be open volumetric receivers, drawing atmospheric air directly into a porous structure. Upscaling window size to the megawatt range will be a challenge. Promising on-sun tests [11, 12, 13] with particle receivers were presented at the SolarPACES 2015 conference, indicating temperatures of 700 °C and higher can be reached. Particle receivers also form part of the current research portfolio at the German Aerospace Centre [14, 15]. An important feature of particle receivers is that they separate the heat transfer fluid from the working fluid in the Brayton cycle, something that is also exploited in this paper.

A few related studies were identified from the literature, although none deal with the case of solar-thermal radiation in optically thin porous media. Kumar and Reddy [16] did a numerical simulation of inclined porous disks inserted inside a transparent cylindrical absorber tube on a parabolic trough collector with thermiol as working fluid. They used constant, but different heat fluxes on the top and bottom half of the tube, and reported a convection heat transfer enhancement of 64 %. They did not include radiation inside the porous medium. Wu and Liou [17] considered radiation transport in a cylindrical tube filled with a scattering medium. They prescribed specular reflection at the tube boundaries, and concluded that there is a strong angular dependence at reflective boundaries. In their investigation the radiation was directed in the axial, not radial direction. Le Dez and Sadat [18] did a similar study for an annular space with semi-transparent walls. Badruddin et al [19] used a thermal non-equilibrium radiation model to predict heat transfer in an annulus filled with an optically thick porous medium with constant temperature boundaries, whilst Fend et al [20] measured the heat transfer properties of an open volumetric receiver experimentally at high fluxes. A direct comparison between our results and the results of these authors is not valid.

We propose a low pressure tubular receiver, but instead of metallic tubes, we suggest the use of transparent quartz glass tubes filled with a porous medium absorber. A staggered tube arrangement ensures a macroscopic volumetric effect, whilst the porous medium fulfils the same function on tube scale. This paper discusses first on sun tests at low concentration ratios and the basic analysis of our concept for a single tube.

CONCEPT DESCRIPTION

The proposed receiver tube [21] comprises of a quartz glass outer tube, and inner metallic tube, and a porous medium filling the annular space between the two tubes, as shown in figure 1. Cold air flows through the inner metallic tube, turns through 180°, and returns through the annular space. The premise is that short wavelength solar radiation will mostly penetrate the quartz glass tube. As a result, the high temperature differences across the tube walls due to conduction are not required. Thus, the outer walls of the quartz tube will be relatively cool, resulting in small conduction and convection losses. Concentrated solar radiation will be absorbed in the porous medium, heating up the matrix structure. This heat is then directly transferred by convection to the air passing through the porous medium. Thermal radiation from the porous medium will be trapped inside the quartz tube, reducing radiation losses.

Anticipated benefits of this configuration are:

- Quartz has a higher operating temperature than most metals.
- Higher incident heat fluxes can be tolerated.
- Radiation and convection losses are small compared to opaque tubes.
- Load bearing components are at low temperature, ensuring structural integrity.
- Free expansion is allowed between inner and outer tubes, reducing thermal stresses.

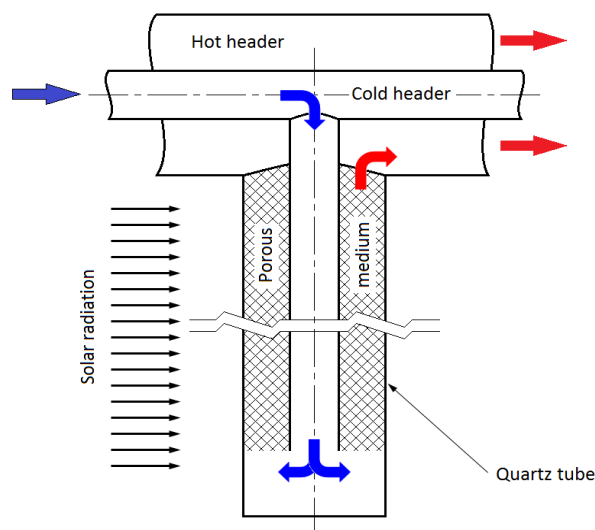


Figure 1. Definition sketch for low pressure receiver tube

Potential draw-backs are:

- Fragility of quartz glass compared to metallic tubes.
- High pressure drop and parasitic load due to the porous medium.
- Fouling of tube surfaces.
- Quartz has a low yield strength compared to metals.

MANIFESTATION

Due to the low yield strength of quartz, and hence the low operating pressure, a Brayton cycle relying on such a receiver directly inside the working fluid will have a low thermal efficiency. However, removing the receiver to a parallel, low pressure stream, and utilizing an air-to-air compact heat exchanger neatly circumvent this problem. A slight modification to the SUNSPOT [1] cycle is suggested to incorporate our receiver, as shown in figure 2.

A blower draws in atmospheric air, and forces it through the receiver tubes, where it is heated to a temperature above 800 °C. This air is passed through a compact heat exchanger, where it transfers its heat to the high pressure air from the compressor. Afterwards, the low pressure air is rejected back into the atmosphere.

A staggered tube arrangement, as shown in figure 3, is proposed for the receiver to create a macro-volumetric effect. Reflected radiation from tube surfaces is partially absorbed by surrounding tubes, rather than being lost to the environment. Deep penetration and a uniform solar heat flux distribution are advantageous towards receiver performance. Heller et al [22] suggested a staggered arrangement with tangential offset between successive tube rows for a hybrid pressure air receiver. They optimised the tangential offset based on a ray-tracing study using SolTrace (Version 2012.7.9) and a known heliostat field. Although their results are applicable to opaque tubes, a similar receiver configuration and design approach is envisaged for this manifestation.

The compressor draws in atmospheric air, and compresses it to about 15 bar. The compressed air is passed through the compact heat exchanger, where it picks up heat from the low pressure stream. It then passes through a combustor, where its temperature is increased to 1 400 °C, before it is expanded through a gas turbine. At present, no practical solution exists to reach the desired turbine inlet temperature on solar operation only. The exhaust gas from the turbine that is at a temperature above 500 °C, is used to charge the rock bed thermal storage.

After sunset, the energy stored during the day is discharged via a steam generator back into the atmosphere. The steam generator supplies steam to a dry-cooled Rankine cycle, allowing the plant to produce electricity continuously over a 24 hour period.

EXPERIMENTAL SET-UP

A manual, dual axis linear Fresnel test rig was designed and built at Stellenbosch University, and on-sun tests were done at the SunRoof Laboratory (GPS coordinates 33.9283 °S, 18.8648 °E) to proof the concept of our receiver. In our tests, we substituted the quartz tube with a 60 mm OD, 50 mm ID borosilicate (Pyrex®) glass tube. The inner tube is a 15 mm copper tube with a wall thickness of 1 mm, whilst the annular space is filled with brass wool (commercial pot scourers). We used spacers to ensure that the copper tube is concentric with the glass tube. Pyrex® glass has a maximum operating temperature of 500 °C, and a maximum working pressure of 11 bar

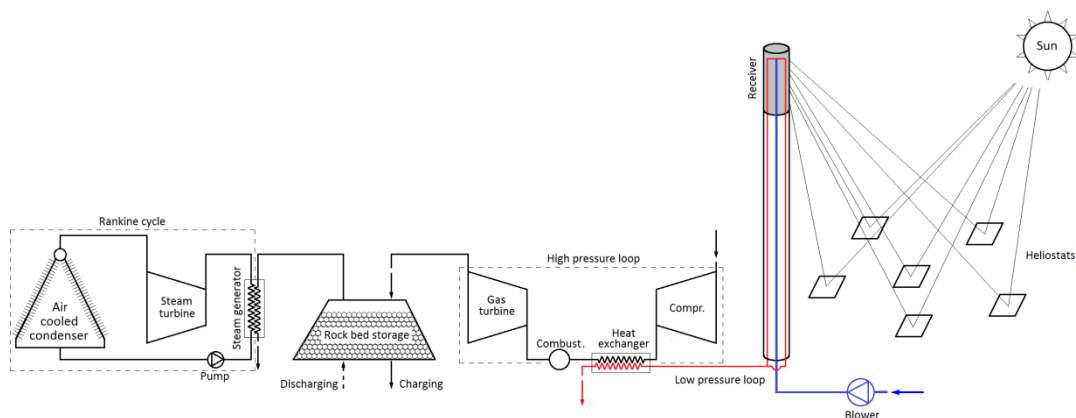


Figure 2. Proposed implementation of low pressure receiver in a modified SUNSPOT cycle



Figure 3. A possible central receiver configuration based upon transparent tubes

at 25 °C. The maximum temperature recorded during test is of the order of 80 °C. The porosity in the annular space is determined from the mass of the brass wool and the volume of the annulus. The average porosity in the annular space is 98 %. The eight mirror linear Fresnel system is mounted on a tilted table, that in turn rests on a rotating base as shown in figure 4 (a). This allows us to direct the long axes of the mirrors normal to the incoming radiation for all tests. We used commercial household glass mirrors, 1.4 m long, 0.1 m wide and 3 mm thick in our test rig. A small bore tube, mounted normal to the tilting table, as shown in figure 4 (b), ensure that the table is facing the sun; if the sun image through the tube deviates from a perfect circle, the tracking angle is manually adjusted. The interval between adjustments is typically 2 minutes.

Service air at 10 bar is available at the test site. The air inlet pressure is controlled to 0.5 bar by a FESTO LRS – QS4 mini pressure regulator. The volume flow rate was measured with an in-line FESTO SFAB-600 rotational flow meter.

We calibrated our thermocouples against a referenced thermocouple in a Fluke calibration machine at 25, 50, 75 and 100 °C. These temperatures were never exceeded during actual testing. The reference thermocouple is calibrated annually.

One temperature measurement is recorded by inserting one thermocouple at the inlet, and twelve at the outlet. This allows us to plot the time dependent temperature profiles at the tube outlet, as well as determine the average temperature increase over the length of the tube. The outer temperature on the outer surface of the glass tube, as well as the axial temperature distribution is measured with a FLIR E60 infrared camera.

EXPERIMENTAL RESULTS AND DISCUSSION

Temperature recordings for thermocouple group 3 from 11:55 to 12:25 on 30 March 2015 is shown in figure 6. It took about 15 minutes to reach a steady state; the first twenty minutes' test data was discarded. Dips in the data correspond to tracking corrections, made every two minutes. The time averaged temperatures for all

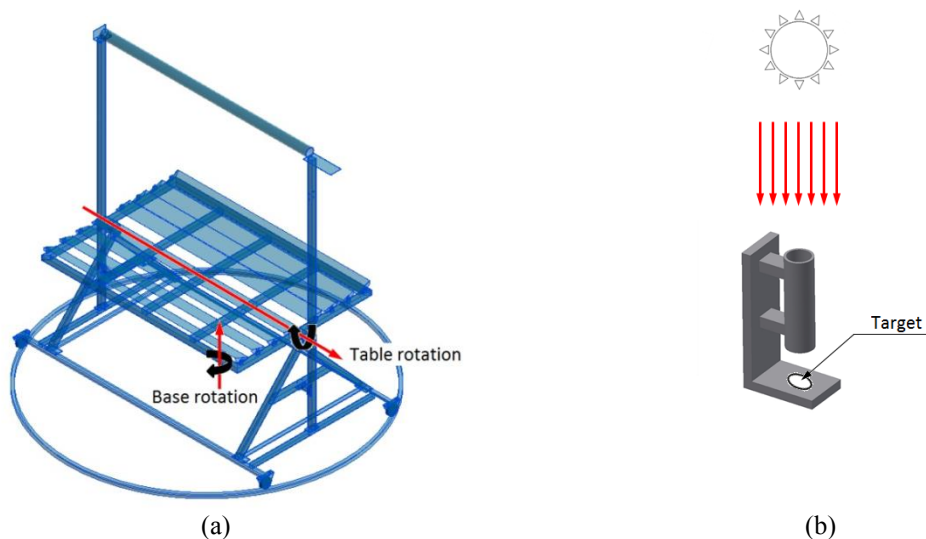


Figure 4. General lay-out of test rig (a), and manual solar tracking indicator (b)

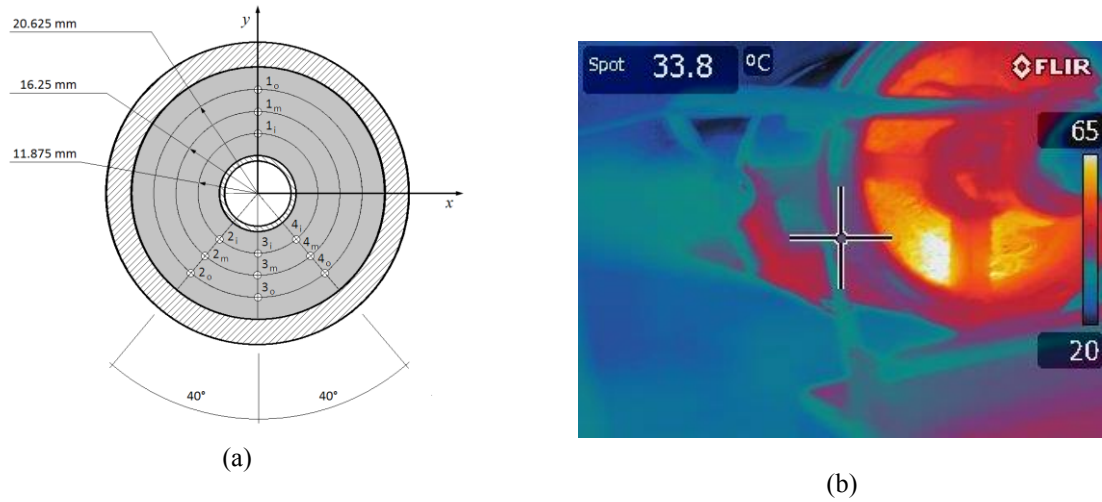


Figure 5. Thermocouple positions (a) and thermal image of tube outlet (b)

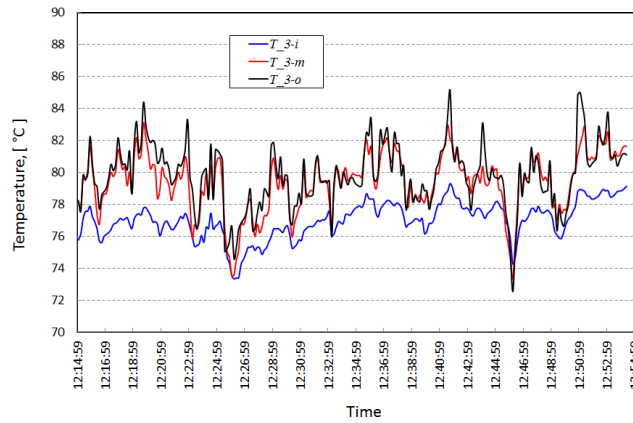


Figure 6. Temperature measurements for thermocouple group 3 during one test

thermocouples are given in table 1. The average direct normal irradiation was $960 \text{ W/m}^2 \pm 0.5 \%$, whilst the average ambient air temperature was $32.0 \text{ °C} \pm 1.3 \%$ and the average wind speed was $2.1 \text{ m/s} \pm 50 \%$ during the test period.

The incident heat flux at the receiver tube was measured with a Vatell TG-1000 flux meter. The bulk of the flux meter made in situ measurements impossible. In order to allow flux measurements, the tube had to be removed. The flux was measured at a single point coincident with the bottom of the glass tube in the same vertical plane as thermocouple groups 1 and 3. Hence, there was a considerable time delay between temperature and flux measurements. The average flux over a 15 minute interval was measured to be 6524 W/m^2 and the 30 minute average DNI value from Sonbesie for the corresponding period was 927 W/m^2 .

The average temperature increase for the air was 34.98 °C at a volume flow rate of $123 \text{ m}^3/\text{min}$. We calculated the receiver efficiency ϵ from

$$\epsilon = \frac{\dot{m}_a c_{pa} (\bar{T}_{ao} - T_{ai})}{\int_0^{2\pi} I_\theta L R d\theta} = 28 \% \quad (1)$$

with \bar{T}_{ao} the area weighted average air outlet temperature, T_{ai} the air inlet temperature, \dot{m}_a the air mass flow rate, c_{pa} its specific heat at the average air temperature, L the tube length, and R the outer radius of the glass tube.

Our measurement system did not allow us to measure the local incident flux I_θ as a function of the circumferential angle θ , only for a spot value directly underneath the tube. We used incident heat flux distribution on the surface of the glass tube from our CFD simulation in the integral. As shown later in this paper, agreement

Table 1. Averaged temperatures measured during a test

Point	$x - x_0$	$y - y_0$	Temperature
	[mm]	[mm]	[°C]
T_{amb}	-	-	31,97
T_{ai}	-	-	39,89
1-i	0,0	11,9	68,94
1-m	0,0	16,3	69,52
1-o	0,0	20,6	64,06
2-i	-7,60	-9,1	74,06
2-m	-10,4	-12,4	77,24
2-o	-13,3	-15,8	77,49
3-i	0,0	-11,9	77,00
3-m	0,0	-16,3	79,38
3-o	0,0	-20,6	79,77
4-i	7,6	-9,1	77,50
4-m	10,4	-12,4	87,19
4-o	13,3	-15,8	85,95

between the CFD prediction and flux measurement at the single point we measured was within 0.4 %.

The receiver efficiency is rather low, largely due to the high porosity and reflection losses from glass. Non-reflective coatings, and using either higher packing densities combined with high emissivity materials in the porous media should improve it substantially.

We measured the pressure loss for cold air across the tube with and without the porous medium. This enabled us to isolate the pressure drop due to the porous medium only. The best fit to our data is given by

$$\frac{\Delta P}{L} = \frac{1}{2} 414.9 \rho v^2 + 292.8 v \tag{2}$$

In equation (2) above, ΔP is the pressure drop in Pascal, L the tube length in m, ρ the mean density of the air in kg/m^3 and v the superficial air velocity through the porous medium in m/s. Near our operating conditions ($v \approx 1.1$ m/s), the viscous and inertial contributions to the total pressure drop are nearly equal. The porous medium contributed less than 2 % to the total pressure drop, mainly a result of the rather high air velocity in the small bore inner tube compared to the velocity through the porous medium itself.

COMPUTATIONAL FLUID DYNAMICS MODEL

Our laboratories are not equipped to measure the optical properties of porous materials. Our workaround was to use a 2-dimensional CFD model to extract the extinction coefficient of the porous medium from the experimental data. Once known, we could use this information in 3-dimensional models in ANSYS Fluent, and also in our own finite difference model (not reported on here).

Consider fully developed flow through a slender annulus filled with a porous medium subject to a constant radiation flux. The steady state energy equation for the air can be written as [25, 26]

$$\rho_a c_{pa} u \frac{d\bar{T}_a}{dx} = \frac{\partial}{\partial x} \left(\psi k_a \frac{\partial T_a}{\partial x} \right) + \frac{1}{r} \frac{\partial}{\partial r} \left(\psi k_a r \frac{\partial T_a}{\partial r} \right) + \frac{1}{r^2} \frac{\partial}{\partial \theta} \left(\psi k_a \frac{\partial T_a}{\partial \theta} \right) + ha(T_s - T_a) \tag{3}$$

with a the contact area between the fluid and matrix per unit volume, ψ the porosity of the medium and u the superficial air velocity. \bar{T}_a is the average air temperature over any cross section through the annulus. For the solid, we have

$$0 = \frac{\partial}{\partial x} \left[(1 - \psi) k_s \frac{\partial T_s}{\partial x} \right] + \frac{1}{r} \frac{\partial}{\partial r} \left[(1 - \psi) k_s r \frac{\partial T_s}{\partial r} \right] + \frac{1}{r^2} \frac{\partial}{\partial \theta} \left[(1 - \psi) k_s \frac{\partial T_s}{\partial \theta} \right] + \dot{Q}_{rad}'''(r, \theta) - ha(T_s - T_a) \tag{4}$$

The radiation source term is a function of the distance ζ traversed by a ray through the porous medium as well as the angle between the beam direction of the radiation and the nodes' position vector.

For large ha , $T_a \approx T_s$, and we can write

$$\frac{1}{r} \frac{\partial}{\partial r} \left(k_{eff} r \frac{\partial T}{\partial r} \right) + \frac{1}{r^2} \frac{\partial}{\partial \theta} \left(k_{eff} \frac{\partial T}{\partial \theta} \right) + \underbrace{\left[\dot{Q}'''(r, \theta) - \rho_a C_{pa} u \frac{d\bar{T}}{dx} \right]}_{\text{Source term}} = 0 \quad (5)$$

since for a constant heat flux, $d\bar{T}/dx$ is constant and $d^2\bar{T}/dx^2 = 0$. The effective conductivity is calculated according to equation (11). Under these conditions, the energy equation is effectively reduced to a two-dimensional heat diffusion equation. We were unable to obtain an analytical solution for equation (5) even for the simple case of simultaneous conduction and radiation in a single tube heated by a collimated beam from the side. In order to determine the extinction coefficient in the porous medium, we opted for a CFD model instead. Our model assumes that the flow is fully developed in the axial direction, and that there is a linear temperature gradient in that direction. Local temperature profiles are the result from thermal radiation and conduction only. Consequently, the CFD model is limited to conduction and radiation transfer. The radiation source term is obtained from solving a separate radiation transport equation in the porous medium. We introduced a volumetric source term to extract energy associated with axial convection from the porous medium. The magnitude of the convective part of the source term was derived from the overall heat balance for our experimental set up. Our experimental data was measured at the tube exit where the flow should be fully developed. We adopted a local thermal equilibrium model in our CFD simulation, as the Sparrow number, as defined by Minkowycz [27] is about 200. We concede that this model might break down near the tube entrance where rather large temperature differences between the matrix and the air are expected.

Thermal radiation in a participating medium is well documented [28, 29, 30, 31]. The discrete ordinates (DO) radiation model in FLUENT is the only radiation model capable of combining multiple radiation bands, specular reflection at the mirrors and participating media in a single model. Due to the high computational demands of the DO model, our hardware constraints limited us to a two-dimensional simulation based on equation (5); a fair approximation of conditions at the tube exit where we measured our experimental values. The extinction coefficient κ was left as a parameter of the solution. The sole purpose of our CFD model was to extract κ from our experimental data. Our measurements do not allow for the separation of the absorption and scattering coefficients. We assumed isotropic scattering, and at first adopted the definitions of the absorption, σ_a , and scattering coefficient, σ_s , for metal foams from Wang et al [31]

$$\sigma_a = \frac{3\varepsilon(1-\psi)}{2d_p} \quad (6)$$

$$\sigma_s = \frac{3(2-\varepsilon)(1-\psi)}{2d_p} \quad (7)$$

with the extinction coefficient κ given by

$$\kappa = \sigma_a + \sigma_s \quad (8)$$

In Wang et al's definition, d_p is the particle (bubble) diameter and ψ the porosity of the medium. In the current application, the only meaningful characteristic length is an effective wire diameter. A unit cell, based on averaging 20 measurements, of the porous medium is depicted in figure 7. Four layers were stacked on top of each other in the radial direction. Assuming that Wang's [31] relationship also holds for wire wool, the ratio between the absorption and extinction coefficients is obtained in terms of the matrix material's emissivity, ε

$$\frac{\sigma_a}{\kappa} = \frac{\varepsilon}{2} \quad (9)$$

With the ratio between the absorption and scattering coefficients fixed, we were able to extract the value of the extinction coefficient from our experimental data.

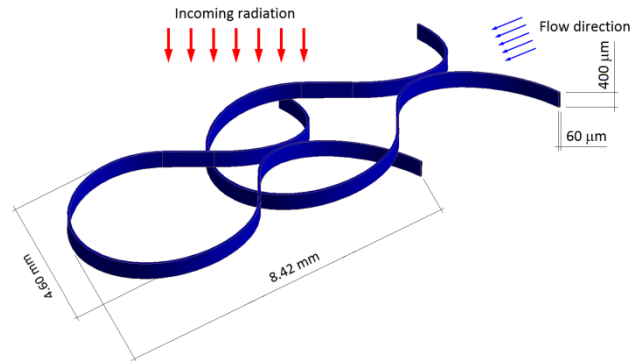


Figure 7. Unit cell structure of porous wool

Initial results were disappointing. Accepting that there are significant differences in the geometry of our wire wool, and the metal foam investigated by Wang et al [31], but retaining their linear relationship between the absorption and scattering coefficients, as stated in equation (9), we opted for the following formulation for the extinction coefficient

$$\kappa = c\sigma_a + (1 - c)\sigma_s; \quad 0 \leq c \leq 1 \quad (10)$$

with c another parameter of our solution. We performed a sensitivity study to obtain the best combination of c and κ that fit our experimental data.

Near the outlet, where we measured temperatures, entrance effects can be neglected. Combined with the high flow resistance of the porous medium, and the near plug flow conditions resulting from it, strong radial and circumferential temperature distributions are expected. The axial temperature distribution should have a negligible effect on the local temperature profile.

The wire diameter ($60 \mu\text{m} \times 400 \mu\text{m}$) is small compared to the annular gap (17.5 mm), allowing us to treat the porous medium as a pseudo-continuous medium [32]. All fluid properties ϕ , except the extinction coefficient, were made up by a first order approximation from contributions by the air and matrix in the relation

$$\phi_{eff} = \psi\phi_{air} + (1 - \psi)\phi_s \quad (11)$$

with ψ the porosity of the medium. Turbulent dispersion will lead to an increase in the apparent conductivity k in a direction perpendicular to the flow direction. Saito and de Lemos [33] suggested a Peclet number based increase over and above the air conductivity, k_a

$$\frac{\Delta k}{k_a} = 0.052(1 - \psi)^{0.5}Pe_d \quad (12)$$

The Peclet number Pe_d is based on the superficial air velocity through the porous medium and the wire diameter. For low porosities and low Peclet numbers, the increase in apparent thermal conductivity is small. Furthermore, for a low conductivity fluid in a high conductivity solid, the effective conductivity is dominated by the contribution from the solid, hence the turbulent dissipation was neglected.

The solid matrix will be at a higher temperature than the air, calling for a thermal non-equilibrium modelling approach [15, 34, 35]. This approach is not compatible with the current implementation in ANSYS Fluent version 16.2.0 [36]. A possible workaround is to define a user defined scalar for the matrix temperature, and solve a separate energy equation for it. The radiative transport equation should be corrected, since the radiation emitted is due to the matrix temperature, T_{solid} , not that of the air T_{air} (that is transparent to radiation). Both temperatures are in Kelvin. Assuming that the absorption coefficient is identical to the emissivity of the matrix material, we have

$$\varepsilon = \sigma_a \left(\frac{T_{solid}}{T_{air}} \right)^4 \quad (13)$$

However, in the current application, actual temperatures are low, the temperature difference between the air and matrix is small due to the low solar magnification, and the large convection heat transfer coefficient, hence $T_{solid}/T_{air} \rightarrow 1$. Thus, a thermal equilibrium model for the porous medium should suffice. Furthermore, we took our readings near the outlet, where temperature and velocity profiles are fully developed and local thermal equilibrium is most likely to be obeyed.

We used borosilicate (Pyrex[®]) glass tubes, rather than quartz in our experiments. Glass is a selective absorber, as shown in figure 8. The cut-off wavelength of $\lambda \approx 2.4 \mu\text{m}$ corresponds to about 97 % of all the radiation emitted by the sun [37]. Consequently, we assumed that 97 % of the direct normal irradiation corresponds to the short wavelength band, with the remaining 3 % in the long wavelength band. The reflective efficiency of the mirrors is 88 % [38].

DISCUSSION OF CFD RESULTS

We adopted a second order DO model for radiation to do the proper implementation in the porous medium, as well as capture the specular reflection from the mirrors. The DO model also enables us to specify multiple wavelength bands, to capture the selective transmissivity of glass. We used one wavelength band for radiation transmitted through the glass, and a long wavelength band for the rest. It does come at the price of much higher computational resources, since the DO model solves a transport equation for each direction and each wavelength band, limiting us to a two dimensional approach. We approximated the spectral absorption properties of the borosilicate glass [40] by two wavelength bands. Eighty five percent of the radiation with wavelengths shorter than $2.4 \mu\text{m}$ is transmitted, whilst the glass is almost opaque to longer wavelengths. A converged solution was reached after increasing the number of DO directions to 180, and using a pixilation of 5×5 , and the resulting radiation flux is shown in figure 9.

A radar plot of the predicted incident heat flux on the surface of the glass tube, represented by the open circles, is shown in figure 10. The open triangles indicate a virtual case where a uniform flux equal to the DNI hits the surface from all directions. It merely serves as a visual indicator to develop a feel for the local concentration ratio. The cross hatched area indicates the receiver tube, and the grey area represents that part of the tube that is shaded from both direct solar radiation, as well as reflected radiation from the mirrors. The incident flux predicted by the CFD model at $\theta = 270^\circ$ is 6547 W/m^2 , compared to the measured heat flux (filled diamond in the figure) of 6524 W/m^2 at the same spot. A maximum incident heat flux is predicted at $\theta = 264^\circ$ measured anti-clockwise from the x -axis, as defined in figure 5 (a). Qualitatively, the agreement with the position of the hot spot in figure 5 (b) is good.

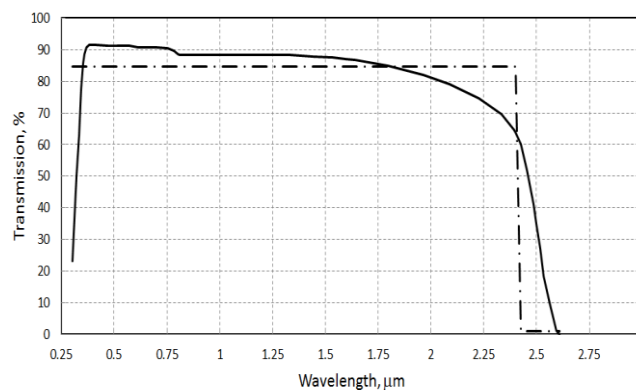


Figure 8. Two-wavelength band approximation (dash-dot-line) of spectral transmissivity (solid line) of Pyrex[®] glass [39]

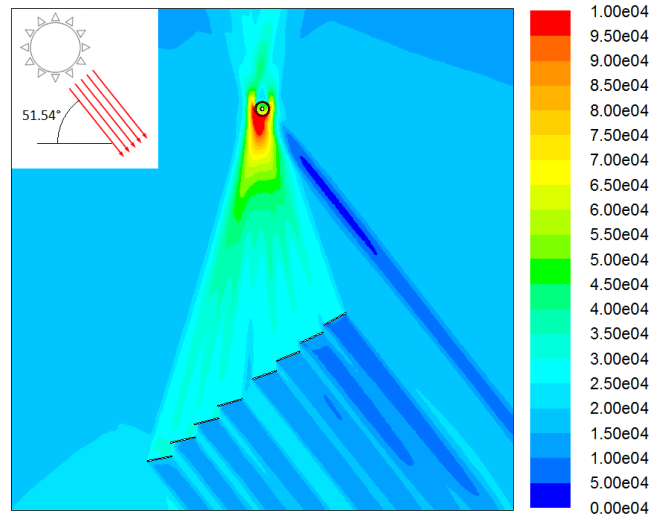


Figure 9. Total incident radiation (total radiation load in all directions passing through a cell [36]) predicted by CFD model

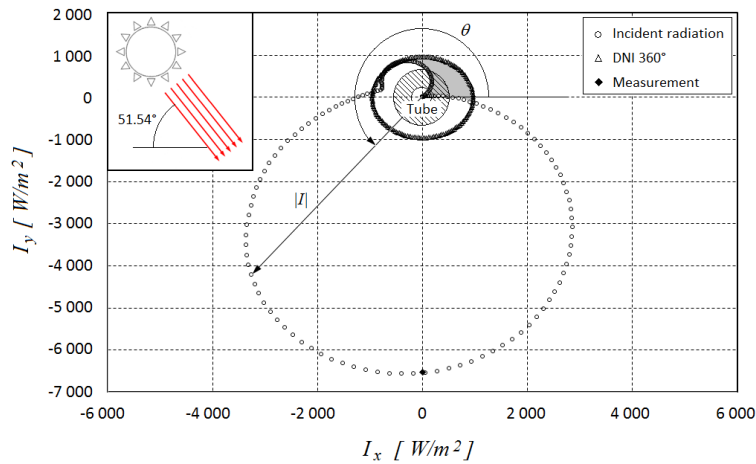


Figure 10. Radar plot of the incident heat flux on the outer surface of the glass tube. Due to the angle definition, the actual direction of incoming radiation is the inverse of arrow direction. Shaded region represent surface of the tube shaded from both direct sunlight and reflected light from the collector

The current version of ANSYS Fluent does not allow one to prescribe a radiation flux at flow inlet boundaries, i.e. the left and right hand borders of the domain shown in figure 9. As a consequence, our CFD model assumes that the test rig is effectively enclosed in a transparent box, since one can prescribe a radiation flux at transparent walls. Due to this restriction, we could only solve the energy and radiation transport equations; heat loss to the environment is by conduction only. A possible workaround would be to adjust the thermal conductivity of the ambient air to match the expected Nusselt number for the stationary case with empirical data mimicking actual convective case. However, this approach does not address the directional effect of forced and free convection, and offers limited value. It was ultimately discarded. In order to estimate the effect of convection, we used correlations from Çengel and Ghajar [37] to estimate the natural and forced convection heat transfer coefficients. For the mixed convection, we adopted

$$h = (h_{nc}^n + h_{fc}^n)^{1/n} \tag{14}$$

A typical value of n would be about 3 - 4 [37]. However, the conduction resistance of the glass tube is an order of magnitude higher than the convection resistance, softening the effect of convection on our temperature readings.

To partially circumvent the convection loss to the environment, we selected experimental data from nearly windless days only, and ignored natural and forced convection losses at the outer surface of the glass tube.

We don't expect that neglecting convection in our CFD model would have a significant impact on our results. We hope future versions of ANSYS Fluent would allow users to specify radiation fluxes at flow inlet or outlet boundaries.

Our two-dimensional CFD model is not 100 % compatible with our three-dimensional experimental set-up. However, the tube length to hydraulic diameter ratio in the porous medium is high. Given that the flow is turbulent, we are of the opinion that the velocity and temperature profiles are fully developed, leading to similarity in the radial temperature distribution along the axis of the tube, especially near the outlet. CFD data for a dimensionless temperature (with T and T_{ave} in °C, the scale was arbitrarily chosen for better resolution in the numerical values of T^*)

$$T^* = \frac{(T - T_{ave})}{T_{ave}} \quad (15)$$

was overlaid on the experimental data, and the value for the extinction coefficient that yield the lowest least squares error fit were adopted as the true extinction coefficient of the porous medium. We defined the error based on the local dimensionless temperature

$$E = \sum_i (T_{CFD,i}^* - T_{exp,i}^*)^2 = f(\kappa, c) \quad (16)$$

with index i referring to the twelve thermocouple positions in figure 5 (a). We were looking to minimize E subject to the constraints

$$\kappa \geq 0 \quad \text{and} \quad 0 \leq c \leq 1 \quad (17)$$

We varied κ and c systematically in our CFD model and assumed that E is a quadratic function of κ and c , a choice inspired by the smooth through shape of our data, but also motivated by the relative expense of generating sufficient data points for a higher order fit. This assumption was eventually borne out by a correlation coefficient of $R^2 = 0.954$.

$$E = a_0 + a_1\kappa^2 + a_2\kappa + a_3\kappa c + a_4c^2 + a_5c \quad (18)$$

Hence, our problem was reduced to finding values for κ and c that simultaneously satisfy

$$\frac{\partial E}{\partial \kappa} = 2a_1\kappa + a_2 + a_3c = 0 \quad (19)$$

$$\frac{\partial E}{\partial c} = 2a_4c + a_5 + a_3\kappa = 0 \quad (20)$$

The best fit to the experimental data was achieved for $\kappa^* = 28.4$ and $c^* = 0.71$. Equations (9) and (10) allow us to reconstruct the absorption and scattering coefficients from our data. Near the optimum, the curvature of E is quite flat and deviations of up to 20 % in the values of κ^* and c^* should have little effect on the predicted radial and circumferential temperature profile in the tube. The minimum value of E lies in a trough of nearly

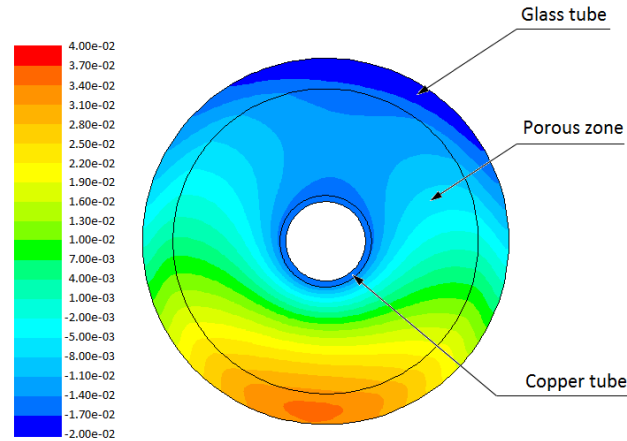


Figure 11. Contour plot of dimensionless temperature T^* from CFD model

constant values of κc (or σ_a), indicating that the CFD model is relatively insensitive to scattering effects. Our data suggests that the contribution by absorption is more pronounced than that suggested by Wang et al [31]. Structurally, our porous wool is vastly different from the cellular structure of their metal foam; hence different optical properties can be expected.

A plot of the relative temperature profile from the CFD model is shown in figure 11. Qualitatively, the temperature profile agrees with the thermal image shown in figure 5(b). The best agreement between CFD and experimental data is observed for thermocouple groups 1 and 3; less so for groups 2 and 4. We did not coat our glass tube with an anti-reflective coating. Inspection of 9 would suggest that beams from the collector mirrors will hit the tube at an oblique angle at these two locations. Reflection of radiation hitting the tube at an oblique angle might partially explain the difference between the experimental and CFD results. Anti-reflective coatings should increase the receiver efficiency [41] substantially. The current version of ANSYS Fluent only allows the user to specify the absorption- and refraction coefficients for the glass, but not boundary conditions at the tube surfaces.

The extinction coefficient is quite low; in the same range as that of glass for short wavelength radiation. This suggests the use of a material with either a lower porosity, or with a closer structure in future work. It might increase the pressure drop across the porous section significantly. Currently, the pressure drop across the porous section is small at 2 % of the total system pressure drop. Even an order of magnitude increase in pressure drop should not render the system infeasible. Our CFD model confirms that higher temperatures can be achieved with higher extinction coefficients, as expected.

CONCLUSION

We presented a low pressure receiver, comprising of a porous medium inside a transparent tube and a manifestation suitable for the SUNSPOT cycle. We have tested a single tube from our receiver at low concentration ratios and have shown that our proposal can work in principle. A fair amount of refinement is still required.

We used an existing linear Fresnel collector, and achieved a modest temperature increase of 40 °C and a receiver efficiency of 28 % at a peak concentration ratio of 7:1. We used a CFD model, assuming isotropic scattering, to analyse the thermal performance of the receiver, with the extinction-, absorption and scattering coefficients parameters of the solution. The extinction coefficient is a linear combination of the absorption and scattering coefficients. We found the best agreement between the experimental and CFD data for $\kappa = 28.4 \text{ m}^{-1}$ and $c = 0.71$ with c a weighting factor of absorption coefficient relative to the extinction coefficient. However, the smallest errors between experimental and CFD data form a trough of almost constant κc . Furthermore, our analyses also indicate that absorption in the porous medium is minimal due to the high porosity, and that the greenhouse effect, rather than volumetric absorption is mostly responsible for the temperature rise. Subsequent analysis suggests that we should increase the packing density in our porous medium to reach higher absorption in the porous layer. It also indicates that the highest temperatures will then move from the glass into the porous medium. In the current configuration, the porous medium is responsible for only 2 % of the total pressure drop, suggesting that we should increase the packing density. This would allow us to increase the packing factor

substantially, without exceeding the limitations set by the mechanical properties of glass or quartz tubes. Fracture mechanics of brittle materials specifically [42], and thermal stress analyses [43, 44] in general are beyond the expertise of the authors and the scope of this paper; we flagged it for further investigation as a potentially limiting factor in the development of our concept.

We did not treat the glass surfaces in any way, and suspect that reflection losses were significant. Applying a non-reflective coating to the glass surface could increase receiver efficiency substantially. Deep inside a tubular receiver, surface reflection might have a positive effect, in that reflected radiation might strike the shaded side of the other tubes, resulting in a more uniform heat flux distribution on tube surfaces.

We are carefully optimistic that we can achieve temperatures above 500 °C with our concept, using higher concentration ratios, proper surface coating/treatment and tailor-made porous media.

In summary:

- We tested a transparent receiver tube with a porous medium in the annular space on a linear Fresnel test bed with a concentration ratio of 7:1.
- The collection efficiency was low (28 %) and the temperature rise about 40 °C at a superficial velocity of 1 m/s.
- Specular reflection at the outer surface of the glass tube had a negative impact on receiver efficiency.
- Absorption in the porous medium was low, and the greenhouse effect dominated it.
- We used a thermal-equilibrium CFD model to extract the extinction coefficient for the porous medium from our experimental data.

ACKNOWLEDGEMENT

This research was sponsored by the Centre for Renewable and Sustainable Energy Studies, Stellenbosch University.

NOMENCLATURE

a	Area density [m^2/m^3]
C_p	Constant pressure specific heat [$\text{J}/\text{kg K}$]
d	Diameter [m]
E	Error
h	Convective heat transfer coefficient [$\text{W}/\text{m}^2 \text{K}$]
I	Incident thermal radiation [W/m^2]
k	Thermal conductivity [$\text{W}/\text{m K}$]
L	Length [m]
\dot{m}	Mass flow rate [kg/s]
P	Pressure [Pa]
R	Radius
r	Radial coordinate
T	Temperature [K or °C]
u	Axial, or x-direction velocity component [m/s]
v	Radial, or x-direction velocity component [m/s]
x	Axial [cylindrical coordinates], or x-direction [Cartesian coordinates] coordinate
y	y-direction coordinate
Δ	Difference
ϵ	Efficiency
ε	Emissivity
θ	Azimuthal coordinate Angle [°]
κ	Extinction coefficient [m^{-1}]
ϕ	Any property
ψ	Porosity
ρ	Density [kg/m^3]

σ_a	Absorption coefficient
σ_s	Scattering coefficient
ζ	Length, [m]

REFERENCES

- [1] D.G. Kröger, The Stellenbosch University solar power thermodynamic cycle, http://sterg.sun.ac.za/wp-content/uploads/2012/10/SUNSPOT_July_20121.pdf, 2012.
- [2] M. Lubkoll, T.W. von Backström, T.M. Harms and D.G. Kröger, Initial analysis on the novel spiky central receiver air pre-heater (SCRAP) pressurized air receiver, Energy Procedia 69, 461 – 470, 2015.
- [3] K.J. Craig, P. Gauché and H. Kretzschmar, CFD analysis of solar tower hybrid pressurized air receiver (HPAR) using a dual-banded radiation model, Solar Energy 110, 338 – 355, 2014.
- [4] L. Heller and P. Gauché, Dual-pressure air receiver cycle for direct storage charging, Energy Procedia 49, 1400 – 1409, 2014.
- [5] L. Heller and J.E. Hoffmann, A cost and performance evaluation of SUNDISC: a dual-pressure air receiver cycle, Energy Procedia 69, 1287 – 1295, 2015.
- [6] A.E. Bergles, 1997, Heat transfer enhancement – the encouragement and accommodation of high heat fluxes, Journal of Heat Transfer, 119, 8 – 19, 1997.